BBA - Bioenergetics 1859 (2018) 411–422

Contents lists available at ScienceDirect

BBA - Bioenergetics

journal homepage: www.elsevier.com/locate/bbabio

YhjA - An *Escherichia coli* trihemic enzyme with quinol peroxidase activity

Cláudia S. Nóbrega[a], Bart Devreese[b], Sofia R. Pauleta[a,*]

[a] Microbial Stress Lab, UCIBIO, REQUIMTE, Departamento de Química, Faculdade de Ciências e Tecnologia, Universidade Nova de Lisboa, Campus da Caparica, 2829-516 Caparica, Portugal

[b] Laboratory of Protein Biochemistry and Biomolecular Engineering, Ghent University, K.L. Ledeganckstraat 35, B-9000 Ghent, Belgium

ARTICLE INFO

Keywords:
Trihemic bacterial peroxidase
Escherichia coli
Oxidative stress
Heme enzyme
Quinol peroxidase activity

ABSTRACT

The trihemic bacterial cytochrome *c* peroxidase from *Escherichia coli*, YhjA, is a membrane-anchored protein with a C-terminal domain homologous to the classical bacterial peroxidases and an additional N-terminal (NT) heme binding domain. Recombinant YhjA is a 50 kDa monomer in solution with three *c*-type hemes covalently bound. Here is reported the first biochemical and spectroscopic characterization of YhjA and of the NT domain demonstrating that NT heme is His63/Met125 coordinated. The reduction potentials of P (active site), NT and E hemes were established to be −170 mV, +133 mV and +210 mV, respectively, at pH 7.5. YhjA has quinol peroxidase activity *in vitro* with optimum activity at pH 7.0 and millimolar range K_M values using hydroquinone and menadiol (a menaquinol analogue) as electron donors (K_M = 0.6 ± 0.2 and 1.8 ± 0.5 mM H_2O_2, respectively), with similar turnover numbers (k_{cat} = 19 ± 2 and 13 ± 2 s^{-1}, respectively). YhjA does not require reductive activation for maximum activity, in opposition to classical bacterial peroxidases, as P heme is always high-spin 6-coordinated with a water-derived molecule as distal axial ligand but shares the need for the presence of calcium ions in the kinetic assays. Formation of a ferryl Fe(IV) = O species was observed upon incubation of fully oxidized YhjA with H_2O_2. The data reported improve our understanding of the biochemical properties and catalytic mechanism of YhjA, a three-heme peroxidase that uses the quinol pool to defend the cells against hydrogen peroxide during transient exposure to oxygenated environments.

1. Introduction

Microorganisms can be transiently or constantly exposed to reactive oxygen species (ROS), namely superoxide ($O_2^{\cdot-}$), hydrogen peroxide (H_2O_2) and hydroxyl radical (HO·), which are the intermediates of the reduction of molecular oxygen to water. These molecules, originated from its own metabolism or from other organisms, are able to cause serious damage to cellular components, such as DNA, proteins and lipids [1]. Therefore, to survive under oxygenated environments, microorganisms developed strategies to detoxify these compounds.

In the case of hydrogen peroxide, this toxic compound is able to diffuse across the membrane [2] and it is continuously formed by auto-oxidation of flavoenzymes in the respiratory chain [1]. Peroxidases and catalases are specialized enzymes that are required by any cell or organism to maintain the concentration of this molecule below toxic levels. Catalases catalyze the disproportionation of hydrogen peroxide, while peroxidases catalyze its reduction by using different reduced compounds (organic molecules or small electron donor proteins). These later enzymes are considered the primary scavengers of H_2O_2 in the cell, which is usually present at the low micromolar range.

In *Escherichia coli*, the most efficient peroxidase is the alkyl hydroperoxide reductase (Ahp [3]), and at high concentrations of hydrogen peroxide, the catalases, KatG [4] and KatE [5], play an important additional role. The contribution of these three enzymes for rapid scavenging of H_2O_2 was in fact confirmed in a triple mutant that showed no scavenging activity [3]. Although, in *E. coli* these three enzymes are the most relevant *in vivo*, there are others with known peroxidase activity that adds complexity to the H_2O_2 scavenging system. These enzymes are the thiol peroxidase (Tpx), bacterioferritin comigratory protein (Bcp) and glutathione peroxidase homologue (BtuE), with YhjA being included in this group of enzymes [6]. YhjA is annotated as a putative cytochrome *c* peroxidase, whose peroxidase activity was not yet clearly demonstrated.

Most of the studies on YhjA were at the genomic level, showing that the promoter region of *yhjA* has a FNR (fumarate and nitrate reduction regulatory protein) and a OxyR binding sites [7], suggesting that its expression would be higher under anaerobic conditions [8] and respond to oxidative and/or nitrosative stress [9,10]. In fact, it was demonstrated that *yhjA* promoter shows higher *lacZ* expression under oxygen-limiting conditions [7]. This led apparently to a controversy since YhjA

* Corresponding author.
E-mail address: srp@fct.unl.pt (S.R. Pauleta).

https://doi.org/10.1016/j.bbabio.2018.03.008
Received 19 October 2017; Received in revised form 11 February 2018; Accepted 13 March 2018
Available online 14 March 2018

would only be present in oxygen-limited environments and oxidative stress derives from oxygen species. However, this is not a unique trait of YhjA. In classical dihemic bacterial cytochrome *c* peroxidases (BCCPs), such as *Neisseria gonorrhoeae* BCCP, its gene expression is also regulated by FNR [11], and thus activated at low oxygen tensions, when the efficiency of the electron transfer pathway for oxidative phosphorylation is low, and thus leakage of electrons to the quinol pool leads to the formation of reactive oxygen species.

Recently, it was shown *in vivo* that YhjA displays significant peroxidase activity in a strain lacking AhpCF, KatG and KatE grown under anaerobic conditions. This activity increased with addition of micromolar concentrations of H_2O_2 to the media. It was proposed that H_2O_2 might be a terminal electron acceptor that allows growth under anaerobic conditions [12].

The analysis of YhjA primary sequence indicates the presence of three *c*-type heme binding motifs (-CXXCH-), and its C-terminal domain, which has two heme binding domains, is homologous to the well characterized classical BCCPs, such as the ones isolated from *Pseudomonas aeruginosa* [13] and *Paracoccus pantotrophus* [14], and from many other bacterial species [15]. The classical BCCPs have a high potential His-Met 6-coordinated heme (E heme) in the C-terminal domain that transfers electrons to a low potential bis-His 6-coordinated heme (P heme) in the N-terminal domain, where the catalytic reaction will occur. In the fully oxidized BCCP, E heme is in a high/low-spin thermal equilibrium due to the loosely bound axial methionine ligand [16], and the P heme is low-spin 6-coordinated. In this state BCCPs are inactive and need reductive activation. This activation mechanism consists in conformational changes mainly at the active site upon reduction of the E heme in the presence of calcium ions. As a consequence, P heme loses its distal histidine ligand and becomes available for hydrogen peroxide binding [17,18]. In this form of the enzyme, at room temperature, P heme has features of a high-spin heme with a characteristic absorption band at 630–640 nm, while at cryogenic temperatures, it displays spectroscopic properties of a low-spin 6-coordinated heme [14,15,18].

Although the gene coding for trihemic BCCPs is found in known pathogenic bacteria [19], these enzymes have been poorly characterized, with homologues only described in *Aggregatibacter actinomycetemcomitans* [20], *Zymomonas mobilis* [21] and *Leptospirillum* spp. [22]. In an iron-oxidizing acidophilic bacterium, *Leptospirillum* spp., the trihemic BCCP gene (*yhjA*) is part of a "*ccp* operon" constituted by *yhjA*, *ahpC* and *perR*, all related to the oxidative stress defense mechanism. According to the authors, this operon is unique to *Leptospirillum* spp. and the encoded BCCP (named CcP) is essential to defend these microorganisms against exogenous H_2O_2 sources and in the early steps of colonization and biofilm formation on metal sulfides [22]. In the case of *Z. mobilis* (PerC) and *A. actinomycetemcomitans* (QPO) trihemic BCCPs, a quinol peroxidase activity has been observed. Furthermore, in *A. actinomycetemcomitans* a null QPO mutant showed higher sensitivity towards H_2O_2 and a lower growth rate under aerobic conditions [23]. In the case of *Z. mobilis*, it was initially suggested that PerC was involved in an incomplete aerobic respiratory pathway, as it lacked a terminal oxidase, but later its role as a quinol peroxidase was recognized [21].

The high sequence homology between YhjA from *E. coli* and homologous enzymes from *Salmonella typhimurium* and *Yersinia pestis* [19] pin points to the importance in understanding the role of this group of enzymes, as well as its enzymatic mechanism, as they can play important roles as virulence trait or be therapeutic targets.

In here, it is presented the first biochemical and spectroscopic characterization of the recombinant soluble YhjA trihemic enzyme. These results aim to understand its catalytic mechanism and the contribution of this enzyme to *E. coli* outstanding resilience towards oxidative stress.

2. Material and methods

2.1. Chemicals

Unless otherwise stated, all reagents were of analytical or higher grade and were purchased from Sigma-Aldrich and Fluka. Ethylene glycol-bis(β-aminoethyl ether)-*N*,*N*,*N*′,*N*′-tetraacetic acid (EGTA) solutions were prepared by addition of 1 M NaOH to bring the pH to 8.0. Solutions were prepared in bi-distilled water or when mentioned in Milli-Q water.

2.2. Bioinformatic analysis

The multi-sequence alignments were performed using the software Mega6.06 [24] with ClustalW [25]. All the analyzed protein sequences were retrieved from the Protein database in NCBI (http://www.ncbi.nlm.nih.gov/protein). Jalview 2.9.0 software was used for sequence representation and consensus analysis [26]. Secondary structure, transmembrane helices and signal peptides were predicted using Jpred 4 (http://www.compbio.dundee.ac.uk/jpred/) [27], TMHMM 2.0 (http://www.cbs.dtu.dk/services/TMHMM-2.0/) [28] and SignalP 4.0 (http://www.cbs.dtu.dk/services/SignalP/) [29], respectively.

2.3. Cloning of YhjA and its domains and protein production

Using *E. coli* K-12 genomic DNA as template, *yhjA* gene was amplified and cloned into a pET22b (+) vector without the region encoding the N-terminal transmembrane domain, to obtain a soluble protein (residues 42–465). Two other clones were prepared, one containing only the N-terminal domain (NT; consisting of the N-terminal *c*-type heme binding domain, residues 42–155) and the other consisting of the C-terminal domain (CT; conserved classical BCCP domain with two *c*-type heme binding sites, comprising residues 171–465). These DNA sequences were amplified with primers that included *Nco*I (N-terminal) and *Xho*I (C-terminal) restriction sites (primers used are presented in Table 1) and cloned into pET22b (+) vectors that confers ampicillin resistance. A N-terminal StrepII-tag with a TEV protease cleavage site for tag removal after purification was added to YhjA. CT and NT domains were cloned with a HisTag at the C-terminal end, which also adds two additional residues (LEHHHHHH). A schematic representation of YhjA constructs prepared for this study are presented in Supplementary information Fig. S2.

E. coli strains TOP10 (Invitrogen) and BL21(DE3) (Novagen) were used for plasmid propagation and protein production, respectively. For

Table 1
Oligonucleotides used in the cloning for protein production. The region encoding for the StrepII-tag is in grey, the recognition site for the TEV is underlined and in bold is the stop codon.

Protein	Primer	Primer Sequence (5'-3')
YhjA	Forward	CAATGCCATGGCTTGGTCTCATCCGCAGTTTGAAAAAGAAAAC
		CTGTATTTTCAGTCTGCTGTCAGTGAAAATAATAAGG
	Reverse	CCAGCTCGAG**TCA**TTGTTTATCCTGCATATACGGC
N-terminal (YhjA_NT)	Forward	CAATGCCATGGCTTCTGCTGTCAGTGAAAATAATAAGG
	Reverse	CCAGCTCGAGGCGCTGTTTTGCAATCC
C-terminal (YhjA_CT)	Forward	CAATGCCATGGCTAATGAACCGGTGCAGCC
	Reverse	CCAGCTCGAGTTGTTTATCCTGCATATACGGC

protein production, *E. coli* BL21(DE3) was co-transformed with the pET22b-*yhjA* variant and pEC86. pEC86 harbors the *ccm* operon to produce all the machinery for *c*-type heme biosynthesis and maturation [30] and confers chloramphenicol resistance. For protein production, four to five colonies of the co-transformed *E. coli* BL21(DE3)/pEC86/pET22b-*yhjA* were used to inoculate 50 mL of LB medium with 100 μg/mL ampicillin and 30 μg/mL chloramphenicol and grown overnight at 210 rpm, 37 °C. Fresh LB medium with the appropriate antibiotics was inoculated with 2% of pre-inoculum. Cells were grown until an $O.D._{600\ nm}$ of 1.5, in an orbital shaker at 210 rpm and 37 °C. At this point, the cells were collected by centrifugation at 3500*g*, 6 °C, 20 min, and re-suspended in half the volume of fresh LB medium with antibiotics. After 1 h incubation at 37 °C and 120 rpm, to stabilize the cells, protein expression was induced with 0.5 mM IPTG at 25 °C for 18 h. The cells were harvested by centrifugation at 7500*g*, 6 °C, 10 min, and re-suspended in 50 mM Tris-HCl, pH 7.6 containing protease inhibitors (cOmplete™, Mini, EDTA-free, Protease Inhibitor Cocktail Tablets, Roche). A similar procedure was used for the other two plasmids, pET22b-*yhjACT* and pET22b-*yhjANT*.

2.4. Purification of YhjA and its domains

The periplasmic fraction was obtained by 5 freeze-thaw cycles and separated from spheroplasts and cell debris by centrifugation at 48000*g*, 6 °C, 15 min. Purification of each protein was performed in two chromatographic steps. In the case of YhjA, the first step was an affinity chromatography, for which a 5 mL StrepTrap column (GE Healthcare) equilibrated with 100 mM Tris-HCl, pH 7.6 and 500 mM NaCl was used. After loading the periplasmic fraction, unbound proteins were eluted with 5 column volumes of equilibration buffer, and afterwards YhjA was eluted with 2.5 mM D-desthiobiotin in the equilibration buffer. The fractions containing YhjA were concentrated over a 5 kDa membrane VivaCell70 (Sartorius) and buffer exchanged to 50 mM Tris-HCl, pH 7.6 and 150 mM NaCl with a desalting PD-10 column (GE-Healthcare). In the second purification step, this fraction was applied onto a gel filtration chromatographic column (HiLoad Superdex 75 16/600, GE Healthcare) equilibrated with 50 mM Tris-HCl, pH 7.6 and 150 mM NaCl. The purity of the fraction during the purification procedure was assessed in a 12.5% SDS-PAGE stained for protein (Coomassie blue) and *c*-type heme content [31]. The fractions were combined, concentrated and desalted using a PD-10 column equilibrated with 20 mM HEPES pH 7.5, and stored at −80 °C in small aliquots until further use.

For both NT and CT domains, the periplasmic fraction was loaded onto a 5 mL HisTrap column (GE Healthcare) equilibrated with 20 mM Tris-HCl, pH 7.6 and 500 mM NaCl. The unbound proteins were eluted with 5-column volumes of equilibration buffer, and afterwards an imidazole step gradient was applied from 0 to 500 mM in equilibration buffer. Both proteins were eluted with 100–200 mM imidazole. The fractions were concentrated over a 5 kDa membrane VivaSpin4 (Sartorius) and buffer exchanged to 20 mM Tris-HCl, pH 7.6 with a desalting NAP-5 column (GE-Healthcare). This fraction was applied onto a 1 mL Resource Q (GE Healthcare) equilibrated with 20 mM Tris-HCl, pH 7.6. An ionic strength gradient from 0 to 500 mM NaCl, in 20 mM Tris-HCl, pH 7.6 was applied and proteins of interest eluted with 100–150 mM NaCl. Proteins were buffer exchanged to 20 mM HEPES pH 7.5, using a NAP-5 column. As before, protein purity was assessed by SDS-PAGE stained for protein and the presence of *c*-type heme (Fig. S4 in Supplementary information), and pure protein samples were stored in small aliquots at −80 °C, until further use.

Total protein and heme content of each protein sample was quantified using the modified Lowry method, with horse heart cytochrome *c* as standard protein [32], and pyridine hemochrome assay, respectively [33].

2.5. Digestion of YhjA Strep-tag by TEV protease

The digestion of Strep-tagged YhjA was performed overnight (20 h), at 4 °C in 50 mM Tris-HCl, pH 8.0, containing 1 mM DTT, 5 mM sodium citrate, 200 mM NaCl and TEV:YhjA in the proportion of 1:20 (mg/mg). The uncut YhjA and the TEV protease were removed by applying the digest onto a tandem 5 mL StrepTrap column and 5 mL HisTrap column (to remove TEV), both equilibrated with 50 mM Tris-HCl, pH 8.0, 500 mM NaCl. The purified digested protein was concentrated, and buffer exchanged to 20 mM HEPES, pH 7.5. 12.5% glycine SDS-PAGE showed a single band with smaller molecular mass (than the uncut protein, data not shown) and size-exclusion chromatogram (Superdex 200 10/300 GL, GE Healthcare) presented one single protein peak. This tag-free YhjA was mainly used in the kinetic assays.

2.6. Molecular mass determination

The molecular mass of all purified proteins was determined by electrospray ionization mass spectrometry (ESI-MS) on a Waters Synapt G1 HDMS mass spectrometer. The apparent molecular weight of the as-isolated protein samples in solution was estimated by molecular size-exclusion chromatography (Superdex 200 10/300 GL, GE Healthcare). The column was equilibrated with 50 mM Tris-HCl, pH 7.6, 150 mM NaCl. The effect of calcium ions on the molecular weight was assessed by either adding calcium ions to the equilibration buffer (2 mM $CaCl_2$) or removing them with 2 mM EGTA. The influence of the ionic strength in the molecular weight was examined by equilibrating the column with 50 mM Tris-HCl, pH 7.6 and 500 mM NaCl. Calibration curves were prepared using the High/Low Molecular Weight Gel Filtration Calibration Kit (GE Healthcare) according to the manufacture instructions. Protein samples were pre-incubated in the respective equilibration buffer for each elution.

2.7. Differential scanning calorimetry

In the differential scanning calorimetry (DSC) experiments, the NanoDSC instrument (TA Instruments) was loaded with degassed buffers (baselines and reference cell) and protein solution (20 μM YhjA in the sample cell). Each protein sample passed through a desalting NAP-5 column (GE Healthcare) equilibrated with 10 mM HEPES pH 7.5, 2 mM $CaCl_2$. The thermograms were acquired at a scan rate of 1 °C/min, from 10 to 100 °C and analyzed with NanoAnalyze software from TA instruments. The corresponding baseline was subtracted from each sample scan and data simulated using a non-two state model to obtain the melting temperature (T_m), the calorimetric (ΔH) and van't Hoff (ΔH_v) enthalpies.

2.8. Spectroscopic characterization – UV–visible and EPR spectroscopies

UV–visible spectra were recorded on a Shimadzu UV-1800 spectrophotometer, connected to a computer, using 1-cm quartz cuvette. The molar extinction coefficients were determined based on heme concentration, considering 3 hemes/protein for YhjA.

YhjA and NT domain were reduced with a solution of sodium ascorbate/diaminodurol (Asc/DAD) to a final concentration of 1 mM and 5 μM, respectively (mixed-valence state). The effect of calcium ions in the visible spectrum of the mixed-valence YhjA was determined by adding $CaCl_2$ to the final concentration of 1 mM. Samples were fully reduced with 5 mM sodium dithionite, prepared in 100 mM HEPES buffer, pH 7.5.

EPR spectra were recorded on a Bruker EMX 6/1 spectrometer equipped with a dual-mode rectangular cavity (Bruker model ER4116DM) and the samples were cooled with an Oxford Instruments ESR900 continuous liquid helium flow cryostat, fitted with a temperature controller, at 10 K. EPR samples of YhjA and NT domain were 0.3 and 0.2 mM, respectively, in 20 mM HEPES buffer, pH 7.5. YhjA

samples were reduced with a solution of Asc/DAD, to a final concentration of 1 mM and 5 μM, respectively, followed by addition of a $CaCl_2$ solution to a final concentration of 2 mM. Experimental conditions for spectra acquisition were: 10 K, 2 mW of microwave power, 5 Gpp of modulation of amplitude, 1×10^5 receiver gain and 3 scans were collected. The spectra simulations were performed using WINEPR SimFonia software version 1.2, from Bruker.

2.9. Redox titration

Potentiometric redox titrations of YhjA and NT domain were performed under argon atmosphere in a MBraun anaerobic chamber, at 25 °C, by measuring the absorption changes of a 6 μM YhjA or NT domain (fully oxidized) in 100 mM HEPES, pH 7.5, 2 mM $CaCl_2$ and 2 μM of each mediator (reduction potentials at pH 7.0 [34]: diaminodurol, +260 mV; 1,2-naphthoquinone, +180 mV; phenazine methosulfate, +80 mV; phenazine ethosulfate, +55 mV; phenazine, −125mV; 2-hydroxy-1,4-naphthoquinone, −145 mV; flavin mononucleotide, −205 mV; neutral red, −325 mV). Throughout the titration, the reduction potential was monitored using a Pt pin electrode combined with an Ag^{1+}/AgCl reference (Crison). The corrected potential relative to the standard hydrogen electrode, was obtained by adding 210 mV. Reductive titration was carried out by stepwise additions of small volumes of 0.1–100 mM sodium ascorbate, or 0.1–100 mM sodium dithionite, prepared in 100 mM HEPES pH 7.5, while the oxidative titration was carried out by addition of 0.1–100 mM potassium ferricyanide.

For each reduction potential, a spectrum was recorded from 350 nm to 900 nm, using a TIDAS diode array spectrophotometer connected to an external computer. By monitoring the 554 nm absorbance of each spectrum, a [oxidized]/[reduced] protein ratio was calculated and plotted as a function of the measured reduction potential. The reduction potentials were obtained from the simulation of the titration curves based on the Nernst equation of one or three independent reduction potentials for NT domain or YhjA, respectively.

2.10. Kinetic assays with $ABTS^{2-}$ and quinol electron donors

The specific peroxidase activity of YhjA was assessed using different electron donors: (i) 2,2′-azino-di-(3-ethyl-benzthiazoline-6-sulphonic acid ($ABTS^{2-}$) oxidation was monitored by the increase in absorbance at 420 nm ($\varepsilon_{420nm} = 36\ mM^{-1}\ cm^{-1}$) over time [35]; (ii) benzene-1,4-diol (hydroquinone) oxidation forming benzoquinone was monitored at 260 nm ($\varepsilon_{260nm} = 5.4\ mM^{-1}\ cm^{-1}$); (iii) 2,3,5,6-tetramethylbenzene-1,4-diol (duroquinol) monitored at 270 nm ($\varepsilon_{270nm} = 19.1\ mM^{-1}\ cm^{-1}$) and (iv) 2-methyl-1,4-naphthalenediol (menadiol) at 260 nm ($\varepsilon_{260nm} = 16.5\ mM^{-1}\ cm^{-1}$). The reduced form of duroquinone and menadione was obtained as described by Giordani and Buc [36]: in short 70 mg of zinc powder was added to 20 mM quinol solution (in 1.7 mL ethanol with 0.18 M HCl), and this solution was degassed and maintained on ice during the assays.

The assays were performed at 25 °C in 10 mM HEPES pH 7.5, 10 mM NaCl and 1 mM $CaCl_2$, containing 3 mM $ABTS^{2-}$ or 100 μM quinol, and 1 mM H_2O_2, and initiated with the addition of as-isolated (oxidized) YhjA (15–30 nM). In the assay for the Michaelis-Menten curve, H_2O_2 concentration ranged from 0.1 to 20 mM. The assays using duroquinol and menadiol were performed with degassed solutions under a constant argon flow to maintain the anoxic conditions.

The observed initial rates, v_{obs}, were determined in the first seconds of the re-oxidation curve, by subtracting the electron donor auto-oxidation rates to determine the real initial rates (Fig. S10, in Supplementary information). A Michaelis-Menten curve was simulated to estimate K_M and V_{max}. The turnover number, k_{cat}, given by $k_{cat} = V_{max} / [YhjA]$, was determined using the concentration of enzyme present in the assay.

The pH dependence of the catalytic activity was assessed in assays performed as described above and varying the buffer, at a concentration of 10 mM buffer, at distinct pH values (MES buffer with pH values from 5.5 to 6.5, HEPES buffer with pH values from 6.5 to 8.0 and Bis-Tris propane buffer with pH values from 8.0 to 9.5). Data were simulated using the following equation derived from a bell-shaped function [37]:

$$v = \frac{v_{max}}{1 + 10^{(pH-pKa)}}$$

in which the reaction rate, v, is given as a function of pH considering one pKa value.

3. Results

3.1. Primary sequence analysis

Analysis of the primary sequence of YhjA in a multiple sequence alignment (Fig. S1 in Supplementary information) indicates the presence of the conserved features of classical BCCPs: calcium binding residues, E heme methionine axial ligand, two heme binding motifs (-CXXCH-), the tryptophan that mediates electron transfer between E and P hemes, and the glutamine and glutamate residues proposed to be involved in the catalytic cycle [15]. The main differences reside in the absence of the histidine residue identified as the P heme distal axial ligand (His87 or His59 in *P. pantotrophus* or *Nitrosomonas europaea*, respectively) and the presence of an additional *c*-type heme binding motif located in the N-terminal domain.

In trihemic BCCPs, the equivalent residue to the mentioned histidine P heme ligand is a hydrophobic residue (Val227, according to *E. coli* numbering), and no conserved histidine seems to be present in the primary sequence of this class of enzymes to fulfill that function. This could suggest that the active site of these enzymes is always high-spin 5-coordinated and available for substrate binding, as previously observed in *N. europaea* BCCP [38], which is active in the oxidized state. Based on the primary sequence alignment, the distal axial ligand of NT heme, can be proposed to be Met125 or His134 (according to *E. coli* numbering), as both residues are conserved in the primary sequence of the trihemic BCCPs analyzed here (Fig. S1 in Supplementary information).

Another unique feature of trihemic BCCPs is the fact that these enzymes are membrane bound, in contrast with the classical BCCPs that are soluble enzymes, with the exception of *N. gonorrhoeae* BCCP that is membrane attached [39]. In fact, the N-terminus of *A. actinomycetemcomitans* QPO was sequenced and corresponds to the first residues of the primary sequence, and a bioinformatic analysis predicted the presence of a transmembrane helix between residues 4 and 26 [20]. A similar analysis of the primary sequence of YhjA by TMHMM 2.0 [28] predicts a transmembrane helix between Ile7 and Asp29 and no signal peptidase cutting site was identified by SignalP. This N-terminal region was removed by the cloning strategy used here to obtain a soluble construct of YhjA.

YhjA is proposed to be able to receive electrons from the quinol pool [12], so the primary sequence of YhjA was also analyzed to identify putative quinol binding sites, for which there are no consensus motifs. However, analysis of the quinol binding pockets in other *E. coli* enzymes, such as fumarate reductase [40] and other membrane associated enzymes, as flavoprotein:ubiquinone oxidorectases [41], shows that residues like aspartate, histidine, tryptophan and tyrosine (among other residues, such as cysteine, arginine and glutamate) play a role in affinity and semiquinone stability. These residues are located in the transmembranar region or in soluble domains of membrane associated proteins. In the YhjA transmembrane helix there are two tyrosines (Tyr19 and Tyr25) and an aspartate residue (Asp30) conserved in all trihemic peroxidase sequences analyzed here, and additionally there are also a cysteine and a histidine residue, which can potentially be involved in quinol binding. In the NT domain, proposed to be in close contact with the membrane (*vide infra*, see Fig. S3 in Supplementary

information), there are few conserved residues (most being *c*-type heme binding motif) but there are three conserved residues that can also play a role in quinol binding (Tyr72, Trp135 and Trp150).

3.2. Heterologous production and biochemical characterization of YhjA and its domains

In order to spectroscopically characterize YhjA, three constructs were prepared: YhjA (soluble version of YhjA without the transmembrane region), NT domain (N-terminal domain binding the additional *c*-type heme) and CT domain (C-terminal domain comprising two heme-binding domains, which is homologous to the classical BCCPs; Figs. S2 and S3A, Supplementary information).

The soluble YhjA (named from now on as YhjA) produced without the transmembrane domain, was successfully purified with a yield of 0.7 mg of pure protein per liter of growth medium and a heme/protein ratio of 3.0 ± 0.1. The molecular mass determined by ESI-MS, 51,070 ± 10 Da, corresponds to the mass of the polypeptide chain of YhjA with 3 *c*-type hemes covalently bound (50,956 Da), without the first residue, the N-terminal methionine, probably due to signal peptide processing, and the addition of one HEPES molecule from the buffer. The heme/protein ratio, as well as the molecular mass determined by mass spectrometry agree with YhjA having three covalently bound hemes.

The NT domain was purified with an average yield of 1 mg of protein per liter and a 0.7 ± 0.1 heme/protein ratio. The molecular mass of 14,770 ± 5 Da agrees with one covalently bound heme per polypeptide chain. The CT domain was a challenge to be properly produced and purified. CT domain production showed a smaller yield compared to the other two constructs (approximately 0.3 mg of pure protein per liter of growth medium) and the molecular mass by mass spectrometry was 33,732 ± 5 Da, which corresponds to the mass of the polypeptide chain without any covalently bound heme. A low heme *c* content (0.2 ± 0.1 heme/protein) in the isolated protein might indicate that there is a small amount of holoprotein but essentially points out that CT domain is mainly produced in the apo-form. The NT and CT domains behave as monomers in solution with 10 ± 2 kDa and 41 ± 2 kDa, respectively (Fig. 1A).

The behavior of YhjA in solution was studied by size-exclusion chromatography and differential scanning calorimetry (DSC). In solution, YhjA behaves as a monomer of 44 ± 2 kDa (I = 200 mM), and the presence or absence of calcium ions (2 mM $CaCl_2$: 42 ± 2 kDa, 2 mM EGTA: 43 ± 2 kDa) or higher ionic strength (I = 550 mM; 40 ± 2 kDa) has no effect in this behavior (Fig. 1A).

Differential scanning calorimetry was used to assess the solution states of YhjA, at pH 7.5. The thermogram for YhjA comprises two overlapping endothermic transitions (Fig. 1B), with *Tm* values of 48.1 ± 0.2 °C and 52.09 ± 0.03 °C and a total calorimetric enthalpy (ΔH_{cal}) of 630 ± 2 kJ/mol, consistent with a monomeric species in solution. These two events can be interpreted as being two unfolding intermediates or the unfolding of two independent domains. The first transition corresponds to one third of the protein sample with a van't Hoff enthalpy of ΔHv_1 = 530 ± 5 kJ/mol, while the second transition accounts for the remaining two thirds of the protein sample and it has a ΔHv_2 = 653 ± 5 kJ/mol. In fact, this later transition has a *Tm* and van't Hoff enthalpy similar to the single transition observed for *P. pantotrophus* BCCP [42] (52.1 °C and ΔHv = 777 kJ/mol) at pH 7.5, in the presence of calcium ions.

Considering the domain organization of YhjA, the first event might correspond to the unfolding of the NT domain, as it is about one third of the protein (15 kDa out of the total 51 kDa), while the second transition can be assigned to the other two thirds of the protein, the CT domain, homologous to classical BCCPs. These separate transitions can reflect different hydrophobicity and flexibility of the NT domain in comparison to the other two domains, which act as a single entity (a single transition has been observed for *P. pantotrophus* and *N. gonorrhoeae* BCCPs, in the presence of calcium ions [42,43]). In fact, secondary structure prediction suggests that there are no structural features (helices or sheets) between the NT and CT domains (residues 150–183) (Fig. S1 in Supplementary information), which might confer some flexibility to the intramolecular interactions between these two domains. The independence of domain unfolding in a multi-domain protein is not unique for this system as it has also been observed in the thermogram of streptokinase, a three domain protein in which the three domains unfold separately with different *Tm* values [44].

3.3. Spectroscopic characterization and reduction potential of the N-terminal domain

YhjA binds three *c*-type hemes, with the two C-terminal ones being homologous of the two hemes of classical BCCPs, which have been well characterized using spectroscopic techniques (including the identification of their axial coordination). The additional N-terminal domain, also containing one *c*-type heme, adds complexity to the visible and EPR spectra of the full enzyme, YhjA. Therefore, to be able to disentangle the contribution of each heme in YhjA, the NT domain was produced as a soluble construct to determine its reduction potential, as well as the distal axial ligand and its spectroscopic properties (Figs. S5 and S6 in Supplementary information).

The visible spectrum of the as-isolated NT domain (Fig. S5A in Supplementary information) has a weak absorption band at 695 nm, which has been attributed to a methionine as axial ligand of a heme iron [45]. The ^{1}H NMR spectrum of the ascorbate-reduced NT domain has well-dispersed and sharp resonances in the H^N region of the spectra (between 6 and 10.5 ppm), with some high-field aliphatic proton resonances also being observed (below 0 ppm, data not shown),

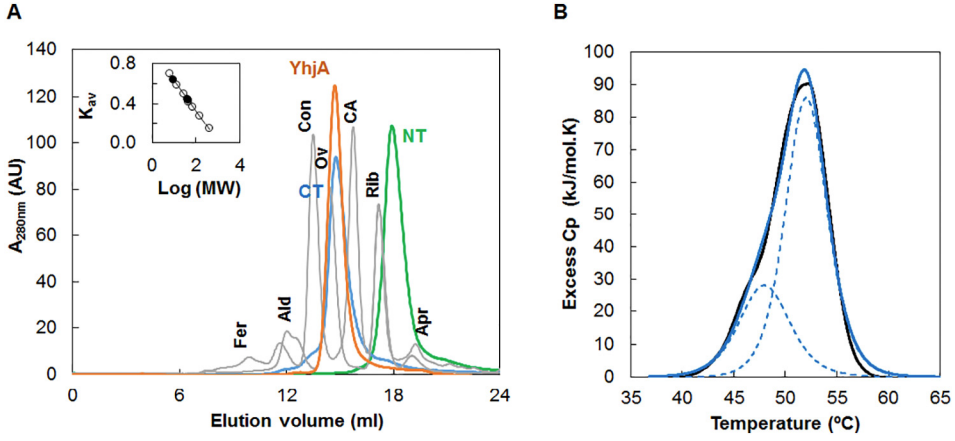

Fig. 1. (A) Elution profile of YhjA (orange line), CT domain (blue line) and NT domain (green line) in the size-exclusion chromatography. In grey are the elution profiles of the standard proteins used to estimate the apparent molecular weight of the proteins: Ferritin (Fer, 440 kDa), Aldolase (Ald, 158 kDa), Conalbumin (Con, 75 kDa), Ovalbumin (Ov, 44 kDa), Carbonic Anhydrase (CA, 29 kDa), Ribonuclease A (Rib, 13.7 kDa) and Aprotinin (Apr, 6.5 kDa). (B) Differential scanning calorimetry of YhjA at pH 7.5 in the presence of calcium ions (black line). The thermograms were baseline corrected and normalized for protein concentration. The simulation fitting the data are represented by a blue solid line, which is the sum of the two independent models (dashed blue lines).

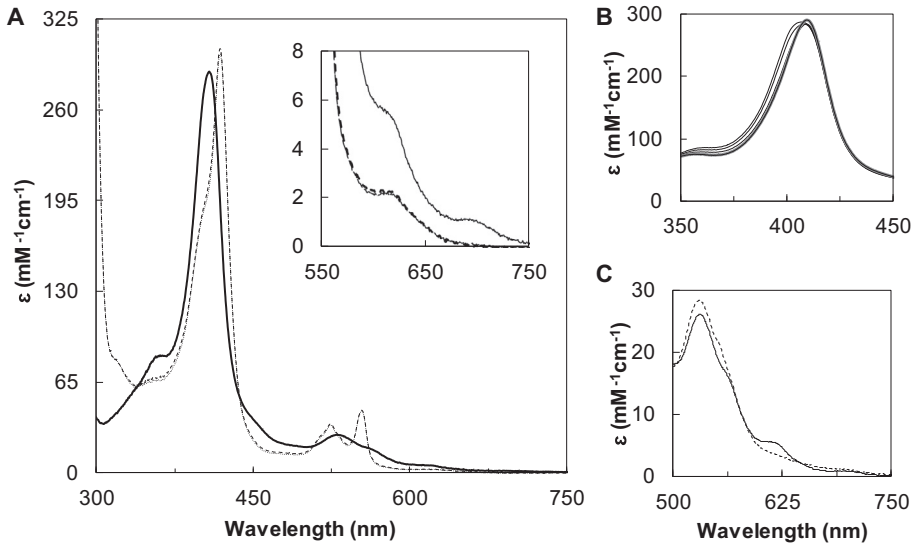

Fig. 2. UV–visible absorption spectra of YhjA, in 10 mM HEPES pH 7.5. (A) The spectrum of the as-isolated YhjA is displayed as a solid line, the dashed and dotted lines are the spectra of mixed-valence and mixed-valence incubated with calcium ions for 10 min, respectively. Inset: High-spin region of the visible spectra in (A). Visible spectra of as-isolated YhjA in the presence of six equivalents of H_2O_2: a shift of the Soret band from 407 to 410 nm is observed in (B) (spectra were recorded at 0, 1, 3, 5 and 10 min after addition of H_2O_2), with concomitant decrease in absorbance at 620 nm and increase in the 510–560 nm region, as presented in (C) (spectra were recorded at 0, continuous line, and 10 min, dashed line, after addition of H_2O_2).

indicative of a well-folded domain. In addition, there is a −2.71 ppm resonance, which is within the range for the chemical shift for the ε-methyl of a methionine residue axially coordinating a heme iron (Fig. S5B in Supplementary information) [46]. Therefore, the additional NT heme is His-Met 6-coordinated, with the axial methionine ligand being most probably the conserved Met125. The EPR spectrum of the oxidized NT domain has characteristics of a low-spin 6-coordinated heme, with *g* values at $g_z = 2.83$, $g_y = 2.38$ and $g_x = 1.52$ (Fig. S5C in Supplementary information). The estimated reduction potential of 55 ± 10 mV is also consistent with a His-Met 6-coordinated *c*-type heme [47] (Fig. S6 in Supplementary information).

3.4. Spectroscopic characterization of YhjA – visible and EPR spectroscopies

The visible spectra of YhjA (Fig. 2) have the typical features of a *c*-type cytochrome absorption spectrum. The Soret band at 407 nm (extinction coefficient of 287 ± 5 $mM^{-1}{\cdot}cm^{-1}$) in the as-isolated form, indicates that all three hemes are oxidized, and the 620 nm band is characteristic of the presence of high-spin hemes. At 695 nm, there is a weak band in the as-isolated spectrum, which has been attributed to a Met axial ligand [45] and also appears in the visible spectrum of the NT domain. In the classical BCCPs this band is usually not observed, as the Met axial ligand of E heme is weakly bound to the heme iron, with E heme being in a high/low-spin temperature dependent equilibrium [16]. Therefore, in the YhjA visible spectrum this band is assigned to the His-Met 6-coordinated NT heme.

The effect of temperature in the spectrum of the as-isolated YhjA between 277 K and 298 K, shows a decrease in the 620 nm absorption band with no increase at 695 nm (Fig. S7 in Supplementary information). This can be explained considering that (i) in this temperature range E heme is not affected (as otherwise an increase in the absorption band at 695 nm would be observed), and (ii) P heme is also in a high/low-spin temperature dependent equilibrium (*vide infra*), contributing to the absorption band at 620 nm.

In the mixed-valence YhjA (reduced with Asc/DAD), there is a shift in the Soret band to 419 nm and the appearance of α- and β-bands at 553 nm and 524 nm, respectively, consequence of the reduction of E and NT hemes (both His-Met coordinated and with a positive reduction potential, *vide infra*). In this spectrum, it is still observed a Soret band of an oxidized heme, as a shoulder at 407 nm, corresponding to the oxidized P heme. The broad absorption band at 620 nm decreases in intensity and is also assigned to P heme that remains in a high-spin configuration (Fig. 2A, inset). P heme is proposed to be 6-coordinated with a water-derived molecule as distal axial ligand, and not 5-coordinated, as could be expected by inspection of YhjA primary sequence (considering the absence in its primary sequence of a putatibe distal histidine ligand or other putative axial ligand), since P heme pocket, being the catalytic site, cannot have a high hydrophobic character as it must be accessible to the substrate and H_2O is the product of the reaction. The identity of the water-derived molecule (either a hydroxide or a water molecule) will be discussed below.

The effect of calcium ions in the visible spectrum of the mixed-valence YhjA was studied using two approaches: (i) addition of $CaCl_2$ (inset in Fig. 2A) and (ii) observing the changes over time by incubating the enzyme with 1 mM EGTA (Fig. S8 in Supplementary information). Upon addition of calcium ions, it was observed a small increase in the absorption band at 620 nm, which is attributed to the high-spin of P heme. After addition of EGTA there is a decrease in intensity of the absorption band at 620 nm.

Although, in classical BCCPs this decrease in absorption at around 620 nm has been interpreted as loss of high-spin and formation of a low-spin species, in YhjA, in the absence of a putative distal axial ligand, a different interpretation must be considered. YhjA's P heme is 6-coordinated with a water-derived molecule as distal axial ligand, exhibiting a high/low-spin thermal equilibrium, with an absorption band centered at 620 nm, at 298 K. Considering that His-OH^- 6-coordinated hemes are low-spin at cryogenic temperatures and high-spin at room temperature, with a broad charge transfer absorption band centered at around 610 nm, while in His-H_2O 6-coordinated hemes this band is centered at 630–640 nm [48,49], YhjA's P heme is proposed to be mainly His-OH^- 6-coordinated, at room temperature.

Therefore, calcium ions might modulate the distal axial ligand p*Ka*, and in its absence an increase in the p*Ka* shifts the equilibrium towards a His-H_2O coordinated heme, with a band at 630–640 nm. The re-distribution of these two populations in the absence of calcium ions is consistent with the apparent decrease in the 620 nm region in the absence of calcium ions. In conclusion, YhjA is purified with the calcium site occupied (this site has a high affinity for calcium ions), since addition of calcium ions to the mixed-valence YhjA produces minor changes in its visible spectrum.

The effect of hydrogen peroxide in the spectrum of the as-isolated YhjA was also studied. It was observed a shift in the Soret absorption band from 407 to 410 nm (Fig. 2B), accompanied by a decrease in the high-spin absorption band at 620 nm, concomitant with an increase at 530 nm (Fig. 2C). Such a shift in the Soret band was also reported in a similar experiment for a *P. aeruginosa* BCCP H71G mutant that, like YhjA, lacks the P heme distal axial histidine ligand, with P heme being available to bind the substrate [50].

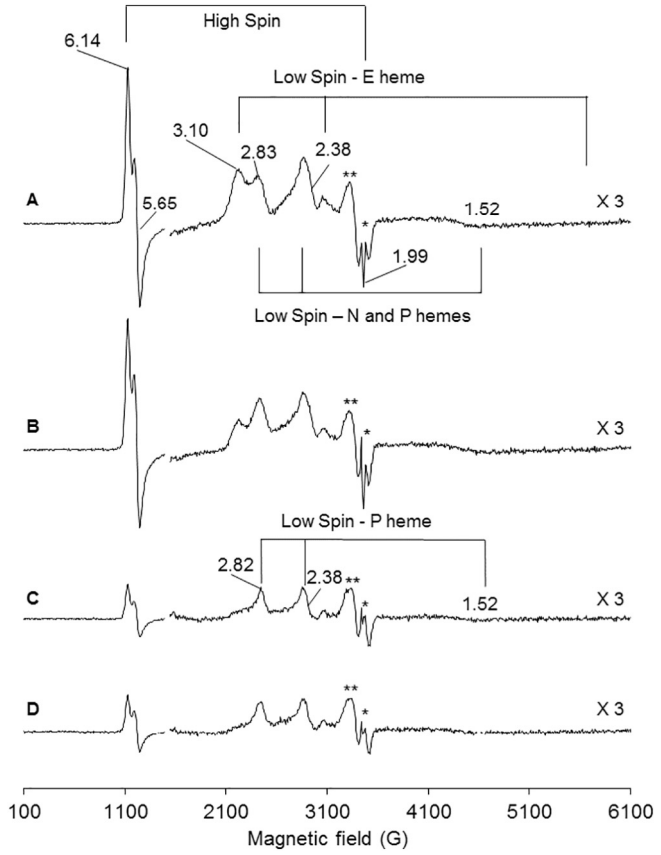

Fig. 3. X-band EPR spectra of YhjA in different oxidation states and effect of calcium ions. Spectra of 0.3 mM YhjA in the as-isolated form (A), after 1 min incubation with Asc/DAD (B), after 60 min incubation with Asc/DAD prior to addition of calcium ions (C) and after 30 min incubation with 2 mM $CaCl_2$ (D). The asterisk (*) marks a radical signal and the double asterisk (**) a signal that was not assigned, both present in all spectra. The low-spin region of the spectra was amplified 3 times.

The EPR spectra of the oxidized and mixed-valence states of YhjA are presented in Fig. 3, with the respective simulations being shown in Fig. S9 in Supplementary information. In the oxidized state, there are two main low-spin signals (Fig. 3A):

i) the signal with $g_z = 3.1$ is attributed to E heme, since after reduction with Asc/DAD for 1 min, it partially disappears (disappearing completely after 60 min) (Fig. 3B). Similar signals, described as Highly Axial Low Spin (HALS) signals, have been found in other *c*-type cytochromes including BCCPs (low-spin E heme signal) from *Shewanella oneidensis* and *Pseudomonas stutzeri* [51,52], even though these type of signals have a $g_{max} \geq 3.2$. This E heme signal is similar to the one observed in *N. europaea* cytochrome c_{552} N64Δ mutant [53], with a broad g_y component, which in the spectra from Fig. 3A is overlapped with the signals from NT and P hemes and was estimated to have a $g_y \sim 2.25$. The third component of the signal should have a $g_x \approx 1.1$, according to the equation for low-spin hemes $g_z^2 + g_y^2 + g_x^2 = 16$ [54], but it is too weak and broad to be observed.
ii) the signal with $g_z = 2.83$ and $g_y = 2.38$ is assigned to both NT and P hemes (two overlapping signals), with the $g_x = 1.52$ being broad and difficult to assign in the spectra of YhjA, but observed in the spectra of the isolated NT domain (Fig. S5C in Supplementary information).

In the mixed-valence YhjA (Fig. 3C), E and NT hemes are reduced and the observed low-spin signal corresponds to P heme. The *g* values of the P heme in these two oxidation states do not change significantly ($g_z = 2.82$ and $g_y = 2.38$) demonstrating that P heme signals were overlapping with the ones of NT heme, and that P heme remains unchanged upon reduction of E and NT hemes. In the classical BCCPs, the *g* values for the bis-His 6-coordinated P heme are approximately $g_z = 3.00$ and $g_y = 2.27$ (in *P. aeruginosa* BCCP [18]) and shift to 2.86 and 2.36, respectively, in the presence of calcium ions. The reduction of E heme in the presence of calcium ions is known to promote the conformational changes that lead to modification in the coordination sphere of P heme, that loses the distal axial histidine ligand. In the case of YhjA, P heme is already 6-coordinated with a hydroxide as distal axial ligand and exhibits a high/low-spin thermal equilibrium, being low-spin at cryogenic temperatures. Thus, P heme coordination does not change with the oxidation state of the enzyme. This agrees with the visible spectra, its temperature dependence and analysis of the primary sequence, which all together indicate that this heme is high-spin 6-coordinated with a hydroxide as distal axial ligand, regardless of the oxidation state of the enzyme, with calcium ions modulating the p*Ka* of this distal axial ligand.

The visible spectra at room temperature showed features of high-spin hemes, which are also present in the EPR spectra at cryogenic temperatures. The EPR spectrum of as-isolated YhjA has a strong high-spin signal with *g* values of 6.14, 5.65 and 1.99, which were assigned to E and P hemes, since NT heme is low-spin at cryogenic temperatures as shown in Fig. S5C in Supplementary information. This signal decreases after 60 min incubation with Asc/DAD, indicating that E heme is contributing to the high-spin component of the as-isolated YhjA EPR spectra. Calcium ions addition to the mixed-valence YhjA (Fig. 3D) slightly changes this high-spin signal, in accordance with the changes observed in the P heme absorption features in the same conditions. This high-spin P heme component might correspond to the small fraction of P heme that is axially coordinated by His-H_2O, at this pH.

Finally, there is a small signal of a radical with a *g* value of ~2, derived from the protein sample, which is present in all the spectra regardless of the condition and oxidation state, overlapping the high-spin signal component (as a note, this radical signal is considerably smaller relative to the other signals). YhjA sample was not pre-incubated with any compound and its structure remains unknown, thus it is not possible to assign this radical signal. Another additional signal with *g* value of 2.04, remains practically unaltered in all spectra and it could not be assigned because there is no EPR signal of a *c*-type heme with such a large component at this *g* value and there are no other signals that could be paired with it. Therefore, it is not possible to assign this signal to either a radical or another species.

3.5. Reduction potentials of YhjA hemes

The CT domain of YhjA is homologous to the classical dihemic BCCPs, thus it is expected to have a high and a low-potential heme, while the redox properties of the additional NT domain were unknown. The reduction potential of each YhjA heme was determined by potentiometric titrations at pH 7.5 (Fig. 4), with the values estimated by fitting the data to the Nernst equation considering three independent redox centers (Table 2).

The comparison between the usual reduction potentials of the two hemes in classical BCCPs with the ones determined in YhjA, led us to assign the reduction potential of +133 ± 10 mV to the NT heme. The difference between the reduction potential of the isolated NT domain (+55 ± 10 mV, see Fig. S6 in Supplementary information) and this value is most likely due to small conformational changes that result in NT heme being more solvent exposed in the isolated truncated NT domain than in the full-length YhjA, making it easier to be oxidized.

The reduction potentials of the three YhjA hemes are more negative than the ones determined for *A. actinomycetemcomitans* QPO, +67 (P), +156 (NT) and +290 mV (E), at pH 7.5 [55]. Although, NT and E heme have similar values, the P heme has a negative reduction

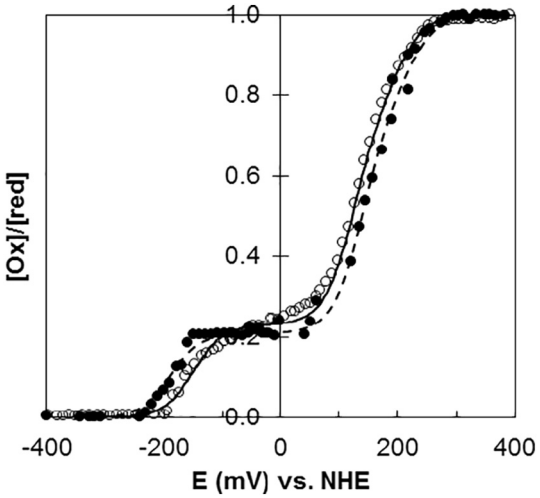

Fig. 4. Potentiometric titration of YhjA at pH 7.5. The reductive titration is represented by open circles and the oxidative titration by closed circles. The lines represent the simulation of the potentiometric curve using the reduction potentials listed in Table 2.

Table 2
Reduction potential of each YhjA heme in the reductive and oxidative titration, at pH 7.5.

	Reduction potentials (mV)		
Direction	P heme	NT heme	E heme
Oxidation	−190 ± 10	140 ± 10	220 ± 10
Reduction	−150 ± 10	125 ± 10	200 ± 10

potential in YhjA, as found in classical BCCPs [19], while in this other enzyme it was determined to be positive.

3.6. Catalytic mechanism - steady state kinetics

The spectroscopic data suggested that YhjA does not need reductive activation since its P heme is high-spin His-OH^- 6-coordinated in the oxidized state and thus it is expected to be able to bind its substrate, hydrogen peroxide, as observed in Fig. 2B and C with formation of an intermediate oxo-ferryl species. This fact was corroborated by the preliminary kinetic data with $ABTS^{2-}$ as electron donor (Fig. S11A in Supplementary information), which showed identical initial rates for the oxidized and mixed-valence state of the enzyme. The calcium dependence of the catalytic activity was assessed for the oxidized form, and without addition of calcium ions to the assay, the initial rates slightly decrease from $0.121 \pm 0.001\,\mu M\,ABTS^{2-}\cdot s^{-1}$ to $0.115 \pm 0.002\,\mu M\,ABTS^{2-}\cdot s^{-1}$. Therefore, YhjA does not require reductive activation but calcium ions are needed to attain maximum peroxidase activity. This trait is different from the one described for *A. actinomycetemcomitans* QPO, which also does not need reductive activation but its activity was not affected by calcium ions removal with EGTA [20].

Four electron donors were used to characterize the peroxidase activity of YhjA: $ABTS^{2-}$, hydroquinone, duroquinol and menadiol, and the respective kinetic parameters for YhjA activity were determined at 25 °C, pH 7.5 (Table 3 and Fig. 5). $ABTS^{2-}$ is an artificial electron donor that has been used as an alternative electron source for classical BCCPs when the physiological electron donor is unknown [56]. Although the turnover number obtained is high, the K_M for $ABTS^{2-}$ is the highest found for the compounds under study (3.7 ± 0.9 mM H_2O_2), making it the most inefficient electron donor tested with the lowest specificity constant (k_{cat}/K_M).

Hydroquinone is the best electron donor with a K_M of 0.6 ± 0.2 mM H_2O_2 and a turnover number of $19 \pm 2\,s^{-1}$, resulting in a specificity constant of $32.2 \pm 0.3\,mM^{-1}\cdot s^{-1}$. This turnover number is similar to $ABTS^{2-}$, k_{cat} of $17 \pm 2\,s^{-1}$ and comparable with the turnover number of *Geobacter sulferreducens* classical BCCP ($15.5\,s^{-1}$) [56].

Table 3
Kinetic parameters obtained for the reduction of hydrogen peroxide by YhjA using different electron donors. All the kinetic parameters were obtained by fitting the kinetic data to a Michaelis-Menten equation.

Electron donor	k_{cat} (s^{-1})	K_M (mM)	k_{cat}/K_M ($mM^{-1}\cdot s^{-1}$)
$ABTS^{2-}$	17 ± 2	3.7 ± 0.9	4.7 ± 0.3
Hydroquinone	19 ± 2	0.6 ± 0.2	32.2 ± 0.3
Duroquinol	12 ± 2	1.2 ± 0.5	9.6 ± 0.4
Menadiol	13 ± 2	1.8 ± 0.5	7.1 ± 0.3

The turnover numbers of duroquinol and menadiol are lower and have similar k_{cat} values, $12 \pm 2\,s^{-1}$ and $13 \pm 2\,s^{-1}$, respectively, but the apparent K_M is lower for duroquinol, which results in an apparent higher specificity. Comparing the oxidation profile of duroquinol with the one of menadiol and hydroquinone, it is clear that the reaction stops after approximately 75 s (Fig. S11B in Supplementary information) even at lower hydrogen peroxide concentrations. Thus, only menadiol and hydroquinone can efficiently transfer electrons to YhjA, maintaining the catalytic activity of the enzyme.

Compared to classical BCCPs, which have K_M values in the micromolar range, YhjA is a poor *in vitro* peroxidase. However, both K_M values and specificity constants are comparable to the quinol peroxidase activity of *E. coli* cytochrome *bd*, a terminal oxidase, which has a K_M of 7 mM and a k_{cat}/K_M of $15\,mM^{-1}\cdot s^{-1}$ [57] for the reduction of hydrogen peroxide.

pH dependence of YhjA peroxidase activity was assessed using hydroquinone as electron donor (Fig. 5C) from pH 5.5 to pH 9.0. YhjA is not stable at lower pH values (5.5–6.5) as it precipitated. The curve was simulated with a p*Ka* of 8.2 ± 0.1 and a maximum activity at pH 7.0. A similar p*Ka* value has been observed in the pH dependence of the activity of classical BCCPs, such as the ones from *N. europaea* and *N. gonorrhoeae*, both with a p*Ka* of 8.4 [43,58].

4. Discussion

4.1. Biochemical characterization of recombinant YhjA

YhjA was successfully expressed and purified as a soluble recombinant form of the enzyme, which enabled its biochemical characterization. This enzyme is a trihemic *c*-type cytochrome, as predicted by the analysis of its primary sequence. Sequence homology indicated that it is a multi-domain protein, with two C-terminal domains homologous to the classical BCCPs, and with an additional N-terminal domain containing also a *c*-type heme.

The classical BCCPs are either dimers or exhibit a monomer-dimer equilibrium dependent on calcium ions and ionic strength [42,52]. On the contrary, YhjA behaves as a monomer of around 44 kDa, with a single monomeric solution state, with the NT domain unfolding almost as a completely independent unit. Given this, it can be proposed that the three domains are not linearly organized, but the N-terminal domain folds towards the C-terminal domains, giving a more globular shape to the protein. In the classical BCCPs the N-terminus is a small helix located at the side of the E heme domain [59], thus the NT domain is most likely closer to this domain (Fig. S3B in Supplementary information).

The spectroscopic characterization of the NT domain enabled the assignment of its distal axial ligand to a conserved methionine residue, Met125. The *c*-type heme in this domain has a reduction potential of +133 mV, in the full length YhjA, which is also in the expected range for a His-Met coordinated *c*-type heme [47]. The spectroscopic properties of the C-terminal domain have similar features to the classical

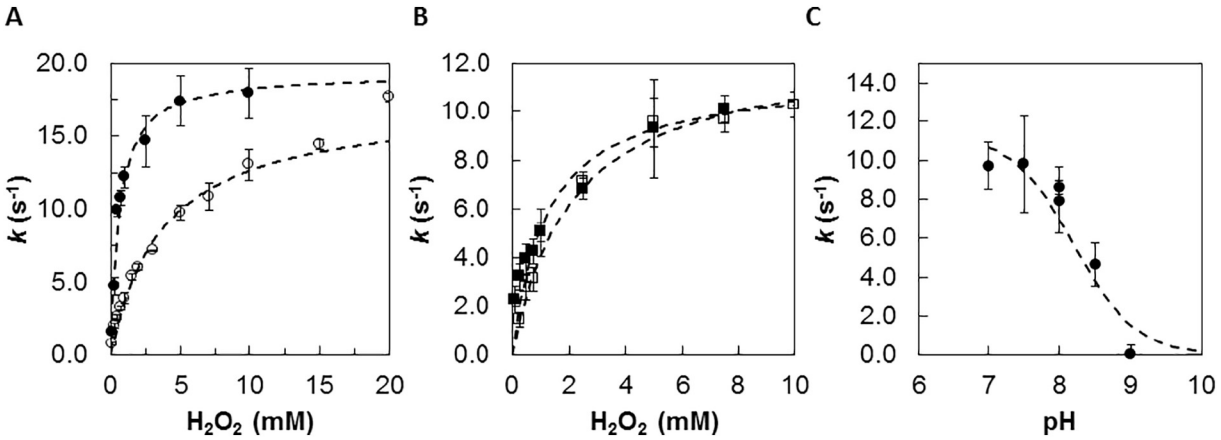

Fig. 5. Steady-state kinetics of YhjA peroxidase activity using $ABTS^{2-}$ (A, open circles), hydroquinone (A, closed circles), menadiol (B, open squares) and duroquinol (B, closed squares). The pH effect on YhjA catalytic activity was assessed with hydroquinone (C). The dashed lines represent the simulated data using the equations in Materials and methods. The results are represented as mean of three replicates and the parameters used in the simulation are the ones listed in the text and in Table 3. YhjA used in the kinetic assays was in the as-isolated form, as described in Materials and methods.

BCCPs, specifically with the one isolated from *N. europaea*, which, is, up-to-date, the only classical BCCP having a high-spin P heme, with an available coordination for substrate binding in both oxidized and mixed-valence state [38].

A Soret shift occurs when the oxidized YhjA is incubated with hydrogen peroxide, which in the oxidized *P. aeruginosa* BCCP mutant without the P heme distal histidine ligand [50], was associated with the formation of an intermediate species at the P heme, the oxo-ferryl (Compound I), followed by formation of a radical species. In other peroxidases similar changes in the spectra were associated with formation of a tryptophan [60] or porphyrin [61] radical. Formation of a porphyrin radical is characterized by a decrease in absorption of the Soret band [61], while the shift in the Soret band is associated with formation of compound II and a tryptophan radical in a horseradish cytochrome *c* peroxidase mutant [60]. In YhjA, the conserved tryptophan (Trp250) between E and P hemes seems to be a good candidate for the radical species, since it could be oxidized by the oxo-ferryl species, as suggested by Hsiao et al. study on *P. aeruginosa* BCCP [50]. Site-directed mutagenesis will be conducted in the future to confirm this and better characterize this radical and the oxo-ferryl intermediate species.

The EPR spectra of a trihemic BCCP are presented here for the first time, showing unique features of the catalytic site (P heme). At cryogenic temperatures, P heme has two distinct states both in the as-isolated and mixed-valence forms: a high-spin 6-coordinated state (possibly distantly coordinated by a water molecule or other weak ligand) and a low-spin hexa-coordinated state with a hydroxide as sixth ligand. The rhombicity of the high-spin P heme signal, in the mixed-valence YhjA EPR spectrum, could on the other hand be due to the presence of one or more weak ligands at cryogenic temperatures. A similar effect was demonstrated by comparison of the EPR spectra and crystal structure of a MauG P107S mutant to the wild-type [62]. This mutant changed the heme cavity (structurally equivalent to P heme) and the heme became coordinated by a weak ligand, Glu113 side-chain, that in YhjA is equivalent to Glu270. The axial high-spin signal observed in the wild-type MauG became rhombic in the P107S mutant. Changes in the YhjA P heme cavity residues might have a similar effect on its EPR spectra.

In conclusion, the spectroscopic properties of YhjA suggest that P heme is 6-coordinated with a hydroxide as distal axial ligand in the oxidized and mixed-valence state of the enzyme, forming an intermediate oxo-ferryl species in the presence of hydrogen peroxide (Fig. 2B and C), which would involve the formation of a protein radical species. Furthermore, His-OH^- 6-coordinated P heme exhibits a high/low-spin thermal equilibrium (being low-spin at lower temperatures) and calcium ions modulate the p*Ka* of its distal ligand. This is supported by the fact that (i) calcium removal by EGTA led to the observation of a re-distribution of two populations: P heme axially coordinated with a water molecule (absorption band at 630 nm) and another with a hydroxide (absorption band at 620 nm), and (ii) at cryogenic temperatures, the component of P heme remaining high-spin, mainly corresponds to the fraction that is His-H_2O 6-coordinated.

The YhjA heme reduction potentials are lower than the ones in the recombinant *A. actinomycetemcomitans* QPO, in particular P heme which in QPO has a positive potential (+67 mV) in contrast to the negative potential (−170 ± 10 mV) found in YhjA and in the classical BCCPs. This might explain the differences in the catalytic cavity of the two enzymes or its positive reduction potential might be due to the presence of detergent (0.5% SM-1200) in their assays, which could affect the protein folding and consequently its redox properties.

4.2. Catalytic activity of the quinol peroxidase YhjA

Other trihemic BCCPs [20,21] display quinol peroxidase activity. Nevertheless, it was reported that *E. coli* overexpressing a recombinant YhjA, had no quinol peroxidase activity using ubiquinol-1 as electron donor [55]. Here, YhjA catalytic activity was analyzed *in vitro* using different quinols and an artificial electron donor, $ABTS^{2-}$. As spectroscopic data indicated, this enzyme is fully active in the oxidized state and needs calcium ions to achieve maximum activity. Thus, YhjA has an active site with an available position for the binding of substrate, which is independent of the oxidation state of the other two hemes, as it was observed that reduction rates in the presence of hydrogen peroxide are similar for both oxidized and mixed-valence YhjA. This trait is a common feature of trihemic BCCPs, as they lack the conserved distal sixth histidine heme ligand in their primary sequence.

YhjA can use quinol as an electron source and of the quinols tested, hydroquinone has proven to be the best electron donor, though it still has a high K_M value. The K_M values are comparable to the one of cytochrome *bd* quinol peroxidase activity *in vitro* [57] but not to the apparent K_M of 5.2 μM H_2O_2 estimated for YhjA *in vivo* [12]. However, it should be noted that in that work, saturating concentrations of substrates were added to the assays, which includes an external source of quinol.

The reason why hydroquinone performs better than duroquinol, even though both are ubiquinol analogues (benzoquinone family) is probably due to its simplicity and lack of ring substituents, such as the four methyl groups in duroquinol ($E^{\circ\prime}$ = +35 mV, pH 7.0 [36]) and ubiquinol ($E^{\circ\prime}$ = +100 mV, pH 7.0 [63]), which translates in hydroquinone having a higher reduction potential ($E^{\circ\prime}$ = +280 mV, pH 7.0 [64]). These properties enable the electron transfer to YhjA

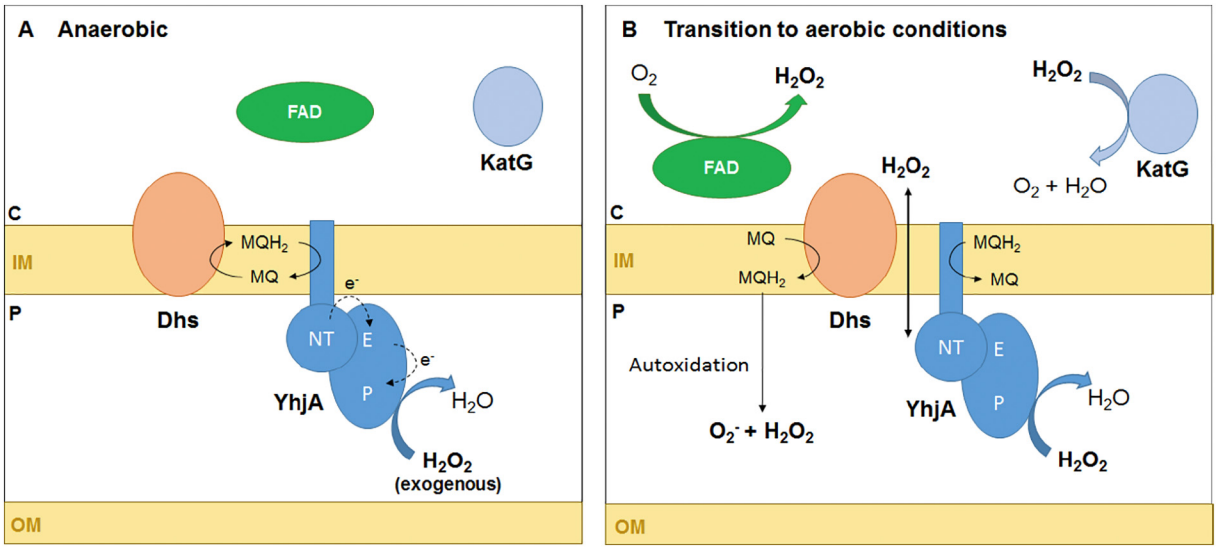

Fig. 6. Proposed model for YhjA role in *E. coli* under anaerobic conditions and when transitioning from an anaerobic to an aerobic environment. (A) Under anaerobic conditions, YhjA reduces H_2O_2 to H_2O using the reductive power of the quinol pool, which is regenerated by dehydrogenases (Dhs). In this scenario H_2O_2 could be considered the terminal oxidant in the absence of other electron acceptors, such as nitrate and fumarate. The electron pathway in YhjA is represented by the dashed arrows, starting from the quinol pool through the NT and E hemes, ending at the active site, the P heme, where the peroxidatic reaction occurs. (B) When cells are first exposed to low oxygen tensions, flavoenzymes (FAD) become significant sources of H_2O_2. The auto-oxidation of quinols, such as menaquinol (MQH_2), also contributes to the increase of ROS. The anaerobically expressed enzymes, KatG and YhjA are the first hydrogen peroxide scavengers. Other significant H_2O_2 sources upon aeration are still not well characterized. C – cytoplasm; P – periplasm; IM – Inner membrane; OM – Outer membrane.

independently of the quinol binding site selectivity (which is absent in the construct used here, *vide supra*) and possibly directly to E heme. Nevertheless, benzoquinones without aromatic ring substituents are not found as physiological quinols and particularly in *E. coli* membranes, the benzoquinone present is ubiquinone [65].

The fact that the quinol binding site might be in the transmembranar region, absent in the YhjA construct used in this study, can explain the lower turnover numbers for duroquinol and menadiol. Nevertheless, duroquinol transferred electrons to YhjA but eventually the reaction stopped, proving to be an inefficient electron donor. On the other hand, menadiol, a menaquinol analogue (naphtoquinone family), which has a single methyl group and a negative reduction potential ($E^{\circ\prime} = -1$ mV, pH 7.0 [36]), does not inhibit the reaction.

In fact, it is likely that YhjA evolved to specifically accept electrons from menaquinol (MQ/MQH_2; $E^{\circ\prime} = -74$ mV) instead of ubiquinol (UQ/UQH_2; $E^{\circ\prime} = +100$ mV) [63], as the main quinols present under anaerobic conditions are the naphthoquinones: demethylmenaquinone and menaquinone [65]. This is in agreement with the recently published data of Khademian and Imlay, in which a Hpx^- *E. coli* strain (lacking the genes *ahpCF*, *katG* and *katE*), unable to produce menaquinone, had lower H_2O_2 scavenging rate under anaerobic conditions [12]. This rate was also comparable to the Hpx^- Δ*yhjA* mutant in the same conditions, corroborating the role of menaquinone as the electron donor of YhjA.

The YhjA catalytic mechanism can be proposed to be similar to the one of classical BCCPs as E and P heme domains are conserved, as well as the tryptophan residue between the two hemes, and it involves an intermediate oxo-ferryl compound with consequent formation of a radical species. Furthermore, a p*Ka* value around 8.5 has also been observed in the catalytic activity of classical BCCPs. This could be associated with the proton transfer required for the release of the second water molecule in the catalytic cycle of these enzymes, which might be mediated by the conserved glutamine at the active site (Gln260). In the mixed-valence classical BCCPs, the side chain of this residue forms a hydrogen bond with the water molecule coordinating the P heme [17] and at higher pH values the proposed proton transfer might be hindered resulting in the decrease of activity that is observed *in vitro*.

The NT heme positive reduction potential and its proximity to the quinol pool make it the likely point of entry of electrons, that are then transferred to E heme. In fact, the most recent work with *A. actinomycetemcomitans* QPO shows that a quinol molecule reduces both NT and E hemes and that the catalytic activity occurs through a Ping-Pong Bi Bi mechanism [66]. Aspects regarding electron transfer pathway will be further explored and clarified when structural data become available.

4.3. In vivo role of YhjA

The auto-oxidation of the quinol pool, specifically menaquinol auto-oxidation when transitioning from anaerobic to aerobic environments, is a source of ROS [67]. A membrane bound quinol peroxidase, such as YhjA would prove to be advantageous in this scenario because not only it would defend the cell against hydrogen peroxide, as it would use the quinol pool, avoiding higher levels of quinol auto-oxidation (Fig. 6B). Other defenses for higher concentrations of H_2O_2 would consist of the cytoplasmic KatG, which is expressed anaerobically. However, given that YhjA is a poor peroxidase, as demonstrated by the kinetic analysis, an alternative role could be as a terminal membrane-bound oxidase, that uses hydrogen peroxide as an anaerobic electron acceptor (Fig. 6A), as suggested by Khademian and Imlay [12].

Furthermore, *yhjA* transcription is FNR-dependent [7,12], which indicates that *E. coli* is capable of adapting its oxidative stress defenses to small variations in oxygen levels, enabling this bacterium to colonize oxygen-limited environments, such as the human gastrointestinal tract. In fact, it was suggested that FNR-dependent regulation allows other intestinal pathogens, from the *Salmonella* and *Shigella* genus (that have a *yhjA* homologous gene in their genome), to infect the epithelial cell layer as the mucosa can present a slightly higher oxygen concentration inducing key virulence factors [68]. In an infection setting, YhjA, from a pathogenic *E. coli* strain, can also play a key role in preparation for cell invasion.

5. Conclusions

This study presents the first biochemical characterization of the trihemic bacterial peroxidase YhjA, one of the enzymes from the large array of hydrogen peroxide scavengers in the *E. coli* oxidative stress system. The as-isolated recombinant YhjA is monomeric and has unique spectroscopic features not found in classical BCCPs, with its peroxidatic

heme having a water-derived molecule as its distal axial ligand and not requiring reductive activation for maximum activity and ability to bind the substrate. The enzyme has quinol peroxidase activity using hydroquinone and menadiol as electron donors. Since duroquinol, an ubiquinol analogue, is not an efficient electron donor and hydroquinone is absent from *E. coli* membranes, we suggest that menaquinol is its physiological electron donor, which agrees with the recent reported data of YhjA being an anaerobically expressed enzyme [12].

The role of YhjA as a peroxidase is unclear in anoxic environments deprived of oxygen species. Unlike strict anaerobes, *E. coli*, a facultative anaerobe, colonizes diverse habitats in which bacteria are likely to encounter oxygen/ROS sources such as, for instance, the human gastrointestinal system. These ubiquitous bacteria have evolved the ability to cope with oxidative stress when faced with oxygenated environments or when pathogenic strains are targeted by the immune system oxidative burst. Their few anaerobic defenses, which would include YhjA, might be sufficient as a first response against these threats, while additional defenses are produced through O_2/ROS-induced pathways.

Author contributions

CSN performed all the experimental data presented, analyzed the data and wrote the manuscript. BD performed the mass spectrometry measurements. SRP designed and planed the project and experiments, contributed to the analysis and discussion of the data and wrote the manuscript.

Transparency document

The Transparency document associated with this article can be found, in online version.

Acknowledgments

This work was supported by Fundação para a Ciência e Tecnologia (FCT) (project grant to SRP, PTDC/BIA-PRO/109796/2009, and scholarship to CSN, SFRH/BD/87878/2012) and by the Belgian Federal Science Policy Office (Belspo) (grant to BD, IAP7/44, iPROS project). Unidade de Ciências Biomoleculares Aplicadas-UCIBIO was financed by national funds from FCT/MEC (UID/Multi/04378/2013) and co-financed by the ERDF under the PT2020 Partnership Agreement (POCI-01-0145-FEDER-007728). The NMR spectrometers are part of the National NMR Infrastructure PT NMR. SRP is an IF fellow supported by FCT.

Appendix A. Supplementary data

Supplementary data to this article can be found online at https://doi.org/10.1016/j.bbabio.2018.03.008.

References

[1] J.A. Imlay, Pathways of oxidative damage, Annu. Rev. Microbiol. 57 (2003) 395–418.
[2] L.C. Seaver, J.A. Imlay, Hydrogen peroxide fluxes and compartmentalization inside growing *Escherichia coli*, J. Bacteriol. 183 (2001) 7182–7189.
[3] L.C. Seaver, J.A. Imlay, Alkyl hydroperoxide reductase is the primary scavenger of endogenous hydrogen peroxide in *Escherichia coli*, J. Bacteriol. 183 (2001) 7173–7181.
[4] A. Hillar, B. Peters, R. Pauls, A. Loboda, H. Zhang, A.G. Mauk, P.C. Loewen, Modulation of the activities of catalase-peroxidase HPI of *Escherichia coli* by site-directed mutagenesis, Biochemistry 39 (2000) 5868–5875.
[5] H.E. Schellhorn, H.M. Hassan, Transcriptional regulation of katE in *Escherichia coli* K-12, J. Bacteriol. 170 (1988) 4286–4292.
[6] S. Mishra, J. Imlay, Why do bacteria use so many enzymes to scavenge hydrogen peroxide? Arch. Biochem. Biophys. 525 (2012) 145–160.
[7] J.D. Partridge, R.K. Poole, J. Green, The *Escherichia coli* yhjA gene, encoding a predicted cytochrome c peroxidase, is regulated by FNR and OxyR, Microbiology 153 (2007) 1499–1507.
[8] G. Unden, S. Achebach, G. Holighaus, H.G. Tran, B. Wackwitz, Y. Zeuner, Control of FNR function of *Escherichia coli* by O_2 and reducing conditions, J. Mol. Microbiol. Biotechnol. 4 (2002) 263–268.
[9] A. Hausladen, C.T. Privalle, T. Keng, J. DeAngelo, J.S. Stamler, Nitrosative stress: activation of the transcription factor OxyR, Cell 86 (1996) 719–729.
[10] M.F. Christman, G. Storz, B.N. Ames, OxyR, a positive regulator of hydrogen peroxide-inducible genes in *Escherichia coli* and *Salmonella typhimurium*, is homologous to a family of bacterial regulatory proteins, Proc. Natl. Acad. Sci. U. S. A. 86 (1989) 3484–3488.
[11] R.N. Whitehead, T.W. Overton, L.A. Snyder, S.J. McGowan, H. Smith, J.A. Cole, N.J. Saunders, The small FNR regulon of *Neisseria gonorrhoeae*: comparison with the larger *Escherichia coli* FNR regulon and interaction with the NarQ-NarP regulon, BMC Genomics 8 (2007) 35.
[12] M. Khademian, J.A. Imlay, *Escherichia coli* cytochrome c peroxidase is a respiratory oxidase that enables the use of hydrogen peroxide as a terminal electron acceptor, Proc. Natl. Acad. Sci. U. S. A. (2017) E6922–E6931.
[13] N. Foote, A.C. Thompson, D. Barber, C. Greenwood, Pseudomonas cytochrome C-551 peroxidase. A purification procedure and study of CO-binding kinetics, Biochem. J. 209 (1983) 701–707.
[14] R. Gilmour, C.F. Goodhew, G.W. Pettigrew, S. Prazeres, I. Moura, J.J. Moura, Spectroscopic characterization of cytochrome c peroxidase from *Paracoccus denitrificans*, Biochem. J. 294 (Pt 3) (1993) 745–752.
[15] G.W. Pettigrew, A. Echalier, S.R. Pauleta, Structure and mechanism in the bacterial dihaem cytochrome c peroxidases, J. Inorg. Biochem. 100 (2006) 551–567.
[16] N. Foote, J. Peterson, P.M. Gadsby, C. Greenwood, A.J. Thomson, A study of the oxidized form of *Pseudomonas aeruginosa* cytochrome c-551 peroxidase with the use of magnetic circular dichroism, Biochem. J. 223 (1984) 369–378.
[17] A. Echalier, C.F. Goodhew, G.W. Pettigrew, V. Fülöp, Activation and catalysis of the di-heme cytochrome c peroxidase from Paracoccus pantotrophus, Structure 14 (2006) 107–117.
[18] A. Echalier, T. Brittain, J. Wright, S. Boycheva, G.B. Mortuza, V. Fülöp, N.J. Watmough, Redox-linked structural changes associated with the formation of a catalytically competent form of the diheme cytochrome c peroxidase from Pseudomonas aeruginosa, Biochemistry 47 (2008) 1947–1956.
[19] J.M. Atack, D.J. Kelly, Structure, mechanism and physiological roles of bacterial cytochrome c peroxidases, Adv. Microb. Physiol. 52 (2007) 73–106.
[20] H. Yamada, E. Takashima, K. Konishi, Molecular characterization of the membrane-bound quinol peroxidase functionally connected to the respiratory chain, FEBS J. 274 (2007) 853–866.
[21] E. Balodite, I. Strazdina, N. Galinina, S. McLean, R. Rutkis, R.K. Poole, U. Kalnenieks, Structure of the *Zymomonas mobilis* respiratory chain: oxygen affinity of electron transport and the role of cytochrome c peroxidase, Microbiology 160 (2014) 2045–2052.
[22] C. Zapata, B. Paillavil, R. Chávez, P. Álamos, G. Levicán, Cytochrome c peroxidase (CcP) is a molecular determinant of the oxidative stress response in the extreme acidophilic *Leptospirillum* sp. CF-1, FEMS Microbiol. Ecol. 93 (2017).
[23] E. Takashima, K. Konishi, Characterization of a quinol peroxidase mutant in *Aggregatibacter actinomycetemcomitans*, FEMS Microbiol. Lett. 286 (2008) 66–70.
[24] K. Tamura, G. Stecher, D. Peterson, A. Filipski, S. Kumar, MEGA6: molecular evolutionary genetics analysis version 6.0, Mol. Biol. Evol. 30 (2013) 2725–2729.
[25] J.D. Thompson, D.G. Higgins, T.J. Gibson, CLUSTAL W: improving the sensitivity of progressive multiple sequence alignment through sequence weighting, position-specific gap penalties and weight matrix choice, Nucleic Acids Res. 22 (1994) 4673–4680.
[26] A.M. Waterhouse, J.B. Procter, D.M. Martin, M. Clamp, G.J. Barton, Jalview version 2—a multiple sequence alignment editor and analysis workbench, Bioinformatics 25 (2009) 1189–1191.
[27] A. Drozdetskiy, C. Cole, J. Procter, G.J. Barton, JPred4: a protein secondary structure prediction server, Nucleic Acids Res. 43 (2015) W389–394.
[28] E.L. Sonnhammer, G. von Heijne, A. Krogh, A hidden Markov model for predicting transmembrane helices in protein sequences, Proc. Int. Conf. Intell. Syst Mol. Biol, 6 1998, pp. 175–182.
[29] T.N. Petersen, S. Brunak, G. von Heijne, H. Nielsen, SignalP 4.0: discriminating signal peptides from transmembrane regions, Nat. Methods 8 (2011) 785–786.
[30] C. Sanders, S. Turkarslan, D.W. Lee, F. Daldal, Cytochrome c biogenesis: the Ccm system, Trends Microbiol. 18 (2010) 266–274.
[31] C.F. Goodhew, I.B. Wilson, D.J. Hunter, G.W. Pettigrew, The cellular location and specificity of bacterial cytochrome c peroxidases, Biochem. J. 271 (1990) 707–712.
[32] G.L. Peterson, Determination of total protein, Methods Enzymol. 91 (1983) 95–119.
[33] E.A. Berry, B.L. Trumpower, Simultaneous determination of hemes a, b, and c from pyridine hemochrome spectra, Anal. Biochem. 161 (1987) 1–15.
[34] P.L. Dutton, Redox potentiometry: determination of midpoint potentials of oxidation-reduction components of biological electron-transfer systems, Methods Enzymol. 54 (1978) 411–435.
[35] R.E. Childs, W.G. Bardsley, The steady-state kinetics of peroxidase with 2,2′-azino-di-(3-ethyl-benzthiazoline-6-sulphonic acid) as chromogen, Biochem. J. 145 (1975) 93–103.
[36] R. Giordani, J. Buc, Evidence for two different electron transfer pathways in the same enzyme, nitrate reductase A from *Escherichia coli*, Eur. J. Biochem. 271 (2004) 2400–2407.
[37] R.A. Alberty, V. Bloomfield, Multiple intermediates in steady state enzyme kinetics. V. Effect of pH on the rate of a simple enzymatic reaction, J. Biol. Chem. 238 (1963) 2804–2810.
[38] H. Shimizu, D.J. Schuller, W.N. Lanzilotta, M. Sundaramoorthy, D.M. Arciero, A.B. Hooper, T.L. Poulos, Crystal structure of *Nitrosomonas europaea* cytochrome c peroxidase and the structural basis for ligand switching in bacterial di-heme peroxidases, Biochemistry 40 (2001) 13483–13490.

[39] S. Turner, E. Reid, H. Smith, J. Cole, A novel cytochrome c peroxidase from *Neisseria gonorrhoeae*: a lipoprotein from a gram-negative bacterium, Biochem. J. 373 (2003) 865–873.
[40] T.M. Iverson, C. Luna-Chavez, L.R. Croal, G. Cecchini, D.C. Rees, Crystallographic studies of the *Escherichia coli* quinol-fumarate reductase with inhibitors bound to the quinol-binding site, J. Biol. Chem. 277 (2002) 16124–16130.
[41] N.J. Watmough, F.E. Frerman, The electron transfer flavoprotein: ubiquinone oxidoreductases, Biochim. Biophys. Acta 1797 (2010) 1910–1916.
[42] G.W. Pettigrew, C.F. Goodhew, A. Cooper, M. Nutley, K. Jumel, S.E. Harding, The electron transfer complexes of cytochrome c peroxidase from *Paracoccus denitrificans*, Biochemistry 42 (2003) 2046–2055.
[43] C.S. Nóbrega, M. Raposo, G. Van Driessche, B. Devreese, S.R. Pauleta, Biochemical characterization of the bacterial peroxidase from the human pathogen *Neisseria gonorrhoeae*, J. Inorg. Biochem. 171 (2017) 108–119.
[44] A.I. Azuaga, C.M. Dobson, P.L. Mateo, F. Conejero-Lara, Unfolding and aggregation during the thermal denaturation of streptokinase, Eur. J. Biochem. 269 (2002) 4121–4133.
[45] E. Shechter, P. Saludjian, Conformation of ferricytochrome c. IV. Relationship between optical absorption and protein conformation, Biopolymers 5 (1967) 788–790.
[46] L. Zhong, X. Wen, T.M. Rabinowitz, B.S. Russell, E.F. Karan, K.L. Bren, Heme axial methionine fluxionality in *Hydrogenobacter thermophilus* cytochrome c552, Proc. Natl. Acad. Sci. U. S. A. 101 (2004) 8637–8642.
[47] Z. Zheng, M.R. Gunner, Analysis of the electrochemistry of hemes with E(m)s spanning 800 mV, Proteins 75 (2009) 719–734.
[48] G. Smulevich, B.D. Howes, E. Droghetti, Structural and functional properties of heme-containing peroxidases: a resonance Raman perspective for the superfamily of plant, fungal and bacterial peroxidases, RSC Metallobiology, 2016, pp. 61–98 (Chapter 4).
[49] V. Fülöp, N.J. Watmough, S.J. Ferguson, Structure and enzymology of two bacterial diheme enzymes: cytochrome cd1 nitrite reductase and cytochrome c peroxidase, Advances in Inorganic Chemistry, Academic Press, 2000, pp. 163–204.
[50] H.C. Hsiao, S. Boycheva, N.J. Watmough, T. Brittain, Activation of the cytochrome c peroxidase of *Pseudomonas aeruginosa*. The role of a heme-linked protein loop: a mutagenesis study, J. Inorg. Biochem. 101 (2007) 1133–1139.
[51] G.S. Pulcu, K.E. Frato, R. Gupta, H.R. Hsu, G.A. Levine, M.P. Hendrich, S.J. Elliott, The diheme cytochrome c peroxidase from *Shewanella oneidensis* requires reductive activation, Biochemistry 51 (2012) 974–985.
[52] C.G. Timóteo, P. Tavares, C.F. Goodhew, L.C. Duarte, K. Jumel, F.M. Gírio, S. Harding, G.W. Pettigrew, I. Moura, Ca^{2+} and the bacterial peroxidases: the cytochrome c peroxidase from *Pseudomonas stutzeri*, J. Biol. Inorg. Chem. 8 (2003) 29–37.
[53] G. Zoppellaro, K.L. Bren, A.A. Ensign, E. Harbitz, R. Kaur, H.P. Hersleth, U. Ryde, L. Hederstedt, K.K. Andersson, Review: studies of ferric heme proteins with highly anisotropic/highly axial low spin (S = 1/2) electron paramagnetic resonance signals with bis-histidine and histidine-methionine axial iron coordination, Biopolymers 91 (2009) 1064–1082.
[54] S. de Vries, S.P. Albracht, Intensity of highly anisotropic low-spin heme EPR signals, Biochim. Biophys. Acta 546 (1979) 334–340.
[55] E. Takashima, H. Yamada, T. Yamashita, K. Matsushita, K. Konishi, Recombinant expression and redox properties of triheme c membrane-bound quinol peroxidase, FEMS Microbiol. Lett. 302 (2010) 52–57.
[56] M. Hoffmann, J. Seidel, O. Einsle, CcpA from Geobacter sulfurreducens is a basic diheme cytochrome c peroxidase, J. Mol. Biol. 393 (2009) 951–965.
[57] S. Al-Attar, Y. Yu, M. Pinkse, J. Hoeser, T. Friedrich, D. Bald, S. de Vries, Cytochrome bd displays significant quinol peroxidase activity, Sci. Rep. 6 (2016) 27631.
[58] A.L. Bradley, S.E. Chobot, D.M. Arciero, A.B. Hooper, S.J. Elliott, A distinctive electrocatalytic response from the cytochrome c peroxidase of *Nitrosomonas europaea*, J. Biol. Chem. 279 (2004) 13297–13300.
[59] V. Fülöp, C.J. Ridout, C. Greenwood, J. Hajdu, Crystal structure of the di-haem cytochrome c peroxidase from *Pseudomonas aeruginosa*, Structure 3 (1995) 1225–1233.
[60] A. Morimoto, M. Tanaka, S. Takahashi, K. Ishimori, H. Hori, I. Morishima, Detection of a tryptophan radical as an intermediate species in the reaction of horseradish peroxidase mutant (Phe-221 → Trp) and hydrogen peroxide, J. Biol. Chem. 273 (1998) 14753–14760.
[61] J.E. Erman, L.B. Vitello, J.M. Mauro, J. Kraut, Detection of an oxyferryl porphyrin pi-cation-radical intermediate in the reaction between hydrogen peroxide and a mutant yeast cytochrome c peroxidase. Evidence for tryptophan-191 involvement in the radical site of compound I, Biochemistry 28 (1989) 7992–7995.
[62] M. Feng, L.M. Jensen, E.T. Yukl, X. Wei, A. Liu, C.M. Wilmot, V.L. Davidson, Proline 107 is a major determinant in maintaining the structure of the distal pocket and reactivity of the high-spin heme of MauG, Biochemistry 51 (2012) 1598–1606.
[63] A.F. Alvarez, C. Rodriguez, D. Georgellis, Ubiquinone and menaquinone electron carriers represent the yin and yang in the redox regulation of the ArcB sensor kinase, J. Bacteriol. 195 (2013) 3054–3061.
[64] H. Nivinskas, S. Staskeviciene, J. Sarlauskas, R.L. Koder, A.F. Miller, N. Cenas, Two-electron reduction of quinones by *Enterobacter cloacae* NAD(P)H:nitroreductase: quantitative structure-activity relationships, Arch. Biochem. Biophys. 403 (2002) 249–258.
[65] G. Unden, J. Bongaerts, Alternative respiratory pathways of *Escherichia coli*: energetics and transcriptional regulation in response to electron acceptors, Biochim. Biophys. Acta 1320 (1997) 217–234.
[66] T. Abe, T. Kawarai, Y. Takahashi, K. Konishi, Enzymatic kinetics of the quinol peroxidase of an aggressive periodontopathic bacterium, J. Biochem. 161 (2017) 513–520.
[67] S. Korshunov, J.A. Imlay, Detection and quantification of superoxide formed within the periplasm of *Escherichia coli*, J. Bacteriol. 188 (2006) 6326–6334.
[68] B. Marteyn, N.P. West, D.F. Browning, J.A. Cole, J.G. Shaw, F. Palm, J. Mounier, M.C. Prevost, P. Sansonetti, C.M. Tang, Modulation of Shigella virulence in response to available oxygen in vivo, Nature 465 (2010) 355–358.